

# Applicability of the Broken-Bond Rule to the Surface Energy of the fcc Metals

I. Galanakis<sup>1</sup>, N. Papanikolaou<sup>2</sup>, and P. H. Dederichs<sup>1</sup>

<sup>1</sup>*Institut für Festkörperforschung, Forschungszentrum Jülich, D-52425 Jülich, Germany*

<sup>2</sup>*Fachbereich Physik, Martin-Luther Universität, Halle-Wittenberg, D-06099 Halle, Germany*

(October 22, 2018)

We apply the Green's function based full-potential screened Korringa-Kohn-Rostoker method in conjunction with the local density approximation to study the surface energies of the noble and the fcc transition and *sp* metals. The orientation dependence of the transition metal surface energies can be well described taking into account only the broken bonds between first neighbors, quite analogous to the behavior we recently found for the noble metals [see cond-mat/0105207]. The (111) and (100) surfaces of the *sp* metals show a jellium like behavior but for the more open surfaces we find again the noble metals behavior but with larger deviation from the broken-bond rule compared to the transition metals. Finally we show that the use of the full potential is crucial to obtain accurate surface energy anisotropy ratios for the vicinal surfaces.

PACS numbers: 71.15.Nc, 71.15.Cr, 71.20.Gj

## I. INTRODUCTION

The surface energy is one of the most fundamental solid state properties since it determines the equilibrium shape of a mesoscopic crystal and plays a decisive role in phenomena like roughening, faceting and crystal growth. Despite of their importance, surface energies are difficult to determine experimentally and just few data exist<sup>1</sup>. Most of these experiments are performed at high temperatures and contain uncertainties of unknown magnitude<sup>1</sup>. The most comprehensive experimental data stem from surface tension measurements in the liquid form being extrapolated to zero temperature<sup>2,3</sup>, which cannot provide orientation specific information. Gold crystallites<sup>4</sup> and single surfaces<sup>5</sup> have attracted a lot of attention aiming to study the orientation dependence of the surface energy, but these experiments, as it was also the case for experiments on In and Pb crystallites<sup>6</sup>, are performed at high temperatures so that the results are difficult to interpret. Entropy terms, describing the lower vibrational frequencies of the atoms at the surface as compared to the bulk, the formation of kinks and finally the creation of holes and pillboxes at the low-index surfaces, have to be added to the total free energy. At such high temperatures the surface-melting faceting<sup>7</sup>, i.e. the break-down of a vicinal surface in a dry and a melted one, plays a predominant role. Also the measurement of core level shifts at the surface has been proposed as an indirect measurement of the surface energy anisotropy<sup>8</sup>. Recently, Bonzel and Edmundts<sup>9</sup> have shown that analyzing the equilibrium shape of crystallites at various temperatures by scanning tunneling microscopy can yield absolute values of the surface energies versus temperature, but this technique has not yet been applied.

During the last years there have been several attempts to calculate the surface energy of metals using either *ab-initio* techniques<sup>10-12</sup>, tight-binding parameterizations<sup>13,14</sup> or semi-empirical methods<sup>15,16</sup>. Methfessel and collaborators were the first to study the trends in the surface energy, work function and relaxation for the whole series of bcc and fcc 4*d* transition metals<sup>10</sup>, using a full-potential version of the linear muffin-tin orbitals (LMTO) method in conjunction with the local-spin density approximation to the exchange-correlation potential<sup>17,18</sup>. In the same spirit Skriver and co-workers have used a Green's function LMTO technique<sup>19</sup> to calculate the surface energy and the work function of most of the elemental metals<sup>11,12,20</sup>. Recently, Vitos and collaborators<sup>22</sup> using their full-charge density (FCD) Green's function LMTO technique in the atomic sphere approximation (ASA)<sup>23</sup> in conjunction with the generalized gradient approximation (GGA)<sup>24</sup> constructed a large database that contains the low-index surface energies for 60 metals in the periodic table<sup>25</sup>. Their results present a mean deviation of 10 % from the full-potential results by Methfessel and collaborators for the 4*d* transition metals<sup>26</sup>. Afterwards, they have used this database in conjunction with the pair-potential model<sup>27</sup> to estimate the formation energy for monoatomic steps on low-index surfaces for an ensemble of the bcc and fcc metals<sup>28</sup>.

In reference 29 we have demonstrated that the surface energies of noble metals scale accurately with the number of broken bonds between first neighbors. This broken-bond rule is very useful for the estimation of the surface energies of vicinal surfaces and of the step energies; the latter ones can be calculated as the energy difference between a vicinal and a flat surface. In this contribution we investigate the question whether the broken-bond rule can also be applied to the surface energies of the other paramagnetic fcc metals: the transition metals Rh, Pd, Ir and Pt, and the *sp*

metals Ca, Sr, Al and Pb. To calculate the surface energies we used the recently developed screened Korringa-Kohn-Rostoker (KKR) method which has been already used to calculate the magnetic properties of  $4d$  monoatomic rows on Ag vicinal surfaces<sup>30</sup>. In Section II we analyze the details of our calculations and the convergence of our results. We also discuss the importance of relativistic effects. In Section III, we present the surface energies of the transition and  $sp$  metals and discuss the applicability of the broken bond rule for these systems. All results presented in section III are obtained accounting for relativistic effects in the scalar-relativistic approximation. Finally we discuss the use of the full-potential instead of the atomic sphere approximation

## II. METHOD OF CALCULATION

### A. Computational Details

To perform the calculations, we used the Vosko, Wilk and Nusair parameterization<sup>31</sup> for the local density approximation (LDA) to the exchange-correlation potential<sup>17</sup> to solve the Kohn-Sham equations within the screened KKR method that was recently developed in our group<sup>32</sup>. Its main advantage is that it can treat both  $2D$  and  $3D$  systems in the same footing. Both the atomic sphere approximation (ASA)<sup>23</sup> and the capability to treat the full-potential (FP) are implemented in this scheme. The ASA calculations take into account the full charge density. It was shown by Andersen and collaborators that the charge density obtained in this way for spherically symmetric potentials is close to the density obtained using a FP method<sup>33</sup>. The full-potential is implemented by using a Voronoi construction of Wigner-Seitz polyhedra that fill the space as described in reference 34. A repulsive muffin-tin potential (4 Ry high) is used as reference system to screen the free-space long-range structure constants into exponentially decaying ones<sup>35</sup>. For the screening we took for all metals interactions up to the second neighbors into account leading to a tight-binding (TB) cluster around each atom of 19 neighbors. To calculate the charge density, we integrated along a contour on the complex energy plane, which extends from the bottom of the band up to the Fermi level<sup>36</sup>. Due to the smooth behavior of the Green's functions for complex energies, only few energy points are needed; in our calculations we used 27 energy points. For the Brillouin zone (BZ) integration, special points are used as proposed by Monkhorst and Pack<sup>37</sup>. Only few tens of  $\mathbf{k}_{\parallel}$  are needed to sample the BZ for the complex energies, except for the energies close to the real axis near the Fermi level for which a considerably larger number of  $\mathbf{k}_{\parallel}$  points is needed. Here we used from  $\sim 300$  points for the vicinal surfaces up to  $\sim 800$  points for the (110) surface. In addition we used a cut off of  $\ell_{max}=6$  for the multipole expansion of the charge density and the potential and a cut off of  $\ell_{max}=3$  for the wavefunctions. Finally in our calculations the core electrons are allowed to relax during the self-consistency.

To simulate the surface we used a slab with  $N$  metal layers and  $N_{vac}$  vacuum layers from each side. We have converged the number of metal and vacuum layers so that our surface energies are converged within 0.01 eV. The number of layers needed to converge the surface energies increases with the roughness of the surface and we had to use 12 layers of the fcc metal for the (111) surface, 14 for the (100), 18 for the (110), 21 for the (311), 30 for the (331) and the (210) surfaces. We have also used 3 vacuum layers from each side of the slab. For all the systems studied we used the experimental lattice parameters: 3.80 Å for Rh, 3.89 Å for Pd, 3.84 Å for Ir, 3.92 Å for Pt, 5.58 Å for Ca, 6.08 Å for Sr, 4.05 Å for Al and finally 4.95 Å for Pb<sup>38</sup>. These numbers differ around 0.1 Å from the numbers used in reference 25 where the theoretical GGA equilibrium lattice constants have been used.

### B. Stability of Anisotropy Ratios

To test our convergence we present in table I the scalar-relativistic ASA low-index surface energies of Ag and the anisotropy ratios with respect to the different parameters used in the program. The absolute values of the energies change less than 0.01 eV and the anisotropy ratios change by less than 1%. The largest effect comes from the  $\ell_{max}$  cut-off for the wavefunctions, but globally the first set of parameters is sufficient to give accurate values of both the surface energies and the anisotropy ratios. The second test presented in table II concerns the effect of the lattice parameter on the surface energies and on the anisotropy ratios. Our test has been also performed for the noble metals in scalar-relativistic ASA. Using Cu as a test case, the absolute values of the surface energies change by the same percentage for all the surface orientations when the lattice parameter is decreased. In the case of Cu the theoretical LDA lattice constant is around 2% smaller than the experimental one, so that this effect changes the surface energy by less than 2.5%. However due to error cancellation the anisotropy ratio changed by less than 1.1%. For Ag and in general for the other  $4d$  metals, Rh and Pd, the LDA lattice constants are somewhat 1% smaller than the experimental lattice constants, while for the  $5d$  metals the LDA values agree with the experimental lattice constants. Therefore the anisotropy ratios are independent of whether we use the LDA or the experimental lattice parameter and the following

discussion of the anisotropy ratios would not change if we would have used the LDA instead of the experimental lattice constants in our calculations.

### C. Relativistic Effects

To study the importance of the relativistic effects we present in figure 1 the non-relativistic (NR) and scalar relativistic (SR) density of states (DOS) for Au and Pt for the central layer atoms of the (111) slab which represent accurately the bulk DOS. Au has all  $d$  states filled and the  $d$ -bands are deeper in energy compared to Pt that has only 9  $d$ -electrons and thus has a peak near the Fermi level. This means that the bonds between Pt atoms are stronger than for Au, so that for Pt more energy is needed to create a surface of a given orientation than for Au. Relativistic effects are small for the Pt DOS at the Fermi level but they widen the  $d$ -band so that the energy needed to break a bond is considerably increased. Although the SR-DOS of Au at the Fermi level is barely enhanced, relativistic effects broaden the band and shift it higher in energy thus enhancing the bonds between Au atoms and increasing the surface energies. Ag and Cu present a similar DOS with Au although the bandwidth of their  $d$ -bands is somehow smaller. In these cases, relativity only slightly changes the DOS, so the effect on the surface energies is smaller than for Au.

In figure 2 we present the FP surface energies of the three noble metals obtained both in NR and SR calculations. The main relativistic effect is to increase the surface energies and this effect is largest for Au being the heaviest element. In the NR calculations Au has the lowest surface energies of all three noble metals but in the SR calculations Au surface energies become comparable to the one of Cu and the inclusion of spin-orbit coupling further increases them<sup>29</sup>. Also the anisotropy ratios are increased compared to non-relativistic values, by about 2-4% in the case of Cu and Ag and up to 8-10% in the case of Au.

## III. SURFACE ENERGIES AND ANISOTROPY RATIOS

We have studied the surface energies of the low-index surfaces, (111), (100) and (110) and of the three most close-packed vicinal surfaces: (311), (331) and (210). From a slab calculation one can calculate the surface excess free energy at zero temperature from the relation

$$\gamma = \frac{E_{slab} - NE_{bulk}}{2} \quad (1)$$

where  $E_{slab}$  is the total energy of the slab,  $N$  is the total number of layers of the metal,  $E_{bulk}$  is the per atom energy in the bulk crystal and the 2 enters because when we do a slab calculation we open two surfaces. To be consistent for all the cases we used as  $E_{bulk}$  the energy per atom of the central layer of the slab.

The broken bond-rule states<sup>29</sup> that the surface energy  $\gamma_{(hkl)}$  in eV/(surface atom) needed to create a surface with a Miller index  $(hkl)$  reduces just to the product of  $\gamma_{(111)}$  and the ratio of the first-neighbor broken bonds  $N_{(hkl)}$  and  $N_{(111)} = 3$ :

$$\gamma_{(hkl)} \cong \frac{N_{(hkl)}}{3} \gamma_{(111)}. \quad (2)$$

$N_{(hkl)}$  can be easily obtained for any fcc surface<sup>39</sup>:

$$N_{(hkl)} = \begin{cases} 2h + k & h, k, l \text{ odd} \\ 4h + 2k & \text{otherwise} \end{cases} \quad h \geq k \geq l. \quad (3)$$

As a consequence the anisotropy ratios between the surface energy for an arbitrary surface orientation over the surface energy for the (111) surface orientation is close to the ratio between the number of broken bonds between nearest neighbors for these surfaces. Here we will study how well the paramagnetic fcc transition and  $sp$  metals satisfy the broken bond rule for the surface energies.

### A. Transition Metals

In table III we have gathered our FP scalar relativistic results for all the transition metal surfaces. The first comment that someone can make on this table is pretty obvious. For all the metals the surface energy increases with

the roughness of the surface, i.e. as the number  $N_{(hkl)}$  of broken bonds increases, where (111) is the most close-packed surface with  $N_{(111)}=3$ . Also it is pretty obvious that surface energies for an isoelectronic row increase with the extent of the wavefunction; the surface energy of Pt is larger than the one of Pd, since the Pt  $5d$  wavefunctions have a somewhat larger extent than the Pd  $4d$  ones. Also along a line surface energy is larger for the compound with the smaller number of  $d$  electrons as this one presents a stronger peak at the Fermi level (see figure 1), e.g. Pt presents larger surface energies than Au. Also in the same table we present in parenthesis the anisotropy ratios. To open the (100) surface we break 4 nearest-neighbor bonds, the (110) 6 bonds, the (311) 7 bonds, the (331) 9 bonds and finally the (210) 10 bonds. So the ideal broken bond ratios with respect to the (111) surface, for which we break 3 nearest-neighbors bonds, are  $4/3$ ,  $2$ ,  $7/3$ ,  $3$  and  $10/3$ , for the (100), (110), (311), (331) and (210) surface orientations respectively. The calculated surface energy anisotropy ratios deviate slightly from these ideal numbers. For Pd the ratios are smaller by the ideal ones by  $\sim 3-4\%$  for all the surface orientations, while Ir ratios are larger from the ideals ones by  $\sim 4-7\%$  for all the surface orientations except the (331) where the Ir calculated ratio is only by  $1.3\%$  larger than the ideal ratio. Pt and Rh show a mixed behavior but in general the ratios differ less than  $3\%$  from the ideal nearest-neighbors broken bonds ratios for any surface. So in general transition metal surfaces follow the broken bond rule but with slightly larger deviations than the noble metals due to the fact that their  $d$  band is not filled and they present peaks at the Fermi level, which can slightly change from one surface orientation to the other and consequently the energy needed to break a bond changes also slightly.

In figure 3 we have plotted the surface energy anisotropy ratios with respect to the (111) surface for the low-index surface together with the results by Vitos *et al.* from the reference 25. In contrast to the noble metals the values of Vitos *et al.* only slightly deviate from our results for the transition metals. In reference 29 we have explained the discrepancy for the noble metals as due to an insufficient number of  $\mathbf{k}_{\parallel}$ -points used in reference 25 in the evaluation of the Brillouin zone integrals. The (111) surface of the noble metals presents a surface state centered at the  $\bar{\Gamma}$  point which can only be accounted for by a sufficiently dense grid. Such states do not occur for the fcc transition metals and thus the number of  $\mathbf{k}_{\parallel}$ -points used in reference 25 is sufficient to produce accurate ratios, that agree well with our FP results. Since the authors of the reference 25 did not perform calculations for the vicinal surfaces, we cannot judge the behavior of the FCD-LMTO-ASA method in these more difficult cases.

As mentioned in the introduction there are several other *ab-initio* calculations for the surface energies of these materials but they concern just one or two surfaces and thus allow no conclusions for the anisotropy ratios. In table IV we have gathered the results from previous *ab-initio* calculations and experiments. We have expressed all the results in  $\text{Jm}^{-2}$  and not in eV/atom, as experiment have been performed in the liquid phase of the metals. For the noble metals our and Vitos' results agree nicely when expressed in  $\text{Jm}^{-2}$ , and the calculated values are very close to the experimental ones. The latter values are not orientation specific but averaged values and they should be closer to the most close-packed surface: the (111). Other calculations agree with our and Vitos databases. The FP-LMTO results by Methfessel and collaborators<sup>10</sup> agree nicely with ours except the case of Ag where they predict a jellium like behavior for the (111) and (100) surfaces, i.e. same surface energy per unit surface area, which is not expected for a noble metal. Finally our calculated surface energies are in reasonable agreement with previous tight-binding calculations by Barreteau *et al.*<sup>13</sup> on the low-index surfaces of Rh and Pd and by Mehl and Papaconstantopoulos<sup>14</sup> on the ensemble of noble and transition metals.

We should mention that in our calculations we did not relax the positions of the layers but to a large extent this effect does not affect the surface energies<sup>29</sup>. Feibelman and collaborators<sup>40,41</sup> and Mansfield and collaborators<sup>42</sup> showed by first-principle calculations that the effect of the relaxation on the calculated surface energy of a particular facet should be around  $2-5\%$  depending on the roughness of the facet. Surface relaxations for vicinal surfaces have been studied mainly using semi-empirical methods due to the complexity arisen by the simultaneous relaxation of a large number of layers<sup>43</sup>. Rodriguez and collaborators using such a semi-empirical method showed that surface relaxations affect typically the anisotropic ratios by less than  $2\%$ <sup>16</sup>, and so the neglect of relaxation should have little effect on our results.

### 1. ASA versus FP Calculations

The results presented in the previous section have been obtained taking into account the non-spherical part of the potential, i.e. known as the full-potential scheme. The use of the FP instead of the ASA accounts in a more accurate way for the charge distribution near the surface where due to the lower symmetry the charge exhibits larger variations than in the bulk. The use of FP lowers the energies compared to ASA by about  $15\%$  for all the surfaces under study. A similar behavior is also found for the vicinal surfaces. At first sight it seems that the ASA is efficiently accurate to describe the surface energies of the materials under study. However, the anisotropy ratios are more sensitive than the surface energies themselves.

In figure 4 we have represented the anisotropy ratios for the noble and transition metals for the three low index and the three vicinal surfaces which we have studied. The straight lines represent the ideal broken bonds ratios. We see that already for the Pd(311) surface the ASA produces a ratio that deviates strongly from the broken bond rule while FP is near it. The differences become even more dramatic for the more open (331) and (210) surfaces. ASA produces ratios for the Cu and Ir surfaces that deviate strongly from the broken bond rule while using the FP we find again the ideal ratios. Especially for Pd, the ASA predicts that the surface energy for the (331) surface is larger than the one for the (210) surface which is more open. The use of FP restores the broken-bond rule behavior. So although the ASA is sufficiently accurate to produce reasonable surface energies, the use of FP is decisive for the calculation of the anisotropy ratios of the vicinal surfaces.

### B. *sp* Metals

To complete our study we also investigated the paramagnetic *sp* metals – Ca, Sr, Al and Pb – that crystallize also in the fcc structure. In table V we have gathered the FP surface energies and in parenthesis the anisotropy ratios for the six more close-packed surfaces. In general the surface energies for these materials are smaller than for the *d* metals due to the fact that the bonds are made of *s* and *p* electrons that are more mobile than the localized *d* electrons and so one needs less energy to break these bonds. This becomes even more clear when we look at the surface energy expressed in surface units (see table VI). The Ca(100) and Sr(100) surfaces show a rather small anisotropy ratio compared to the transition and noble metals and also compared to Al. Ca and Sr are in the periodic table just near the simple metals which are known to be well described by a simple jellium model<sup>44</sup>. So we expect that to some extent we would find a jellium like behavior also for the Ca and Sr surfaces at least for the low-index ones. This is really what happens. In figure 5 we represent the anisotropy ratios but now taking into account the energy per surface area ( $\text{Jm}^{-2}$ ) and not per atom (eV/atom). For a jellium model the surface energy per surface area would be constant for any surface and the anisotropy ratio would be always 1. With the solid line we represent the anisotropy ratios if the broken-bond rule is applicable, and the ratios for Ca, Ag and Ir. Ag is closer to the broken bond rule than Ir where the ratios are always overestimated. For the Ca(100) surface we see that the value is closer to the jellium model but for the more open surfaces the anisotropy ratios are closer to the broken bond model than the jellium.

Contrary to Ca and Sr, Al shows the same behavior with Pd and the calculated ratios are slightly smaller than the ideal ones (see table V). The most interesting case is Pb. For the (100) and (110) surfaces the ratios are near the Sr ones while for the next two vicinal surface orientations, (311) and (331), the calculated anisotropy ratios are more than 6% smaller than the ideal values. But for the (210) surface the anisotropy ratio changes the behavior and now is larger by 6% than the ideal value of 10/3. This is an indication that the behavior of Pb is more complicated than all the other fcc metals we have studied in this contribution. Here we have to mention that the surface energies in table V have been calculated taking the *5d* as valence electrons as they are located just below the *sp* bands. We recalculated the surface energies of Pb considering the *5d* as core states, by increasing the number of layers, the number of energy points used to do the integrations in the complex energy plane and finally the number of  $\mathbf{k}_{\parallel}$ -points. Although the surface energies changed slightly due to the core treatment of the *5d* states, the anisotropy ratios were extremely stable.

In table VI we have gathered our calculated surface energies in  $\text{Jm}^{-2}$  together with other calculations and experiments. Our results agree nicely with the Vitos *et al.* database in reference 25 with the exception of Pb where our surface energy per surface area is double as high, but our results agree nicely with previous calculations by Mansfield and Needs<sup>42</sup> using pseudopotentials and the existing experimental data. Both Schöchlin *et al.*<sup>45</sup> and Stumpf and Scheffler<sup>46</sup> have studied all the three low-index surfaces of Al. Comparing Schöchlin *et al.* calculations with Stumpf's and Scheffler's results we see that the former calculations predict comparable surface energies for the (100) and (110) surfaces while the latter ones predict comparable surface energies for the (111) and (100) surfaces. Both calculations are in contradiction to our calculations that predict a considerable increase of the surface energy as the surface becomes more open, while the calculations in reference 25 state that the surface energy per surface area is smaller for the (110) surface compared to the (100) surface. This spread of the results for Al does not allow us to draw safe conclusions for the variation of the surface energy with the surface orientation.

## IV. CONCLUSIONS

We have shown using the full-potential (FP) screened KKR code that the broken bond rule, i.e. the surface energy scales linearly with the number of nearest-neighbors broken bonds, already shown for the noble metals is also valid for the transition metals. For the *sp* metals the (111) and (100) surfaces show a jellium like behavior but for the more

open surfaces the surface energies follow again the broken-bond rule with Pb presenting the largest deviations. The use of full-potential instead of the full-charge atomic-sphere approximation (ASA) decreased the surface energies and we showed that it is necessary to accurately calculate the anisotropy ratios for the vicinal surfaces.

## ACKNOWLEDGMENTS

Authors gratefully acknowledge support from the TMR network of *Interface Magnetism* (Contract No: ERBFMRXCT96-0089) and the RT Network of *Computational Magnetoelectronics* (Contract No: RTN1-1999-00145) of the European Commission.

- 
- <sup>1</sup> V.K. Kumikov and Kh.B. Khokonov, *J. Appl. Phys.* **54** (1983) 1346.  
<sup>2</sup> W.R. Tyson and W.A. Miller, *Surf. Sci.* **62** (1977) 267.  
<sup>3</sup> F.R. Boer, R. Boom, W.C.M. Mattens, A.R. Miedema, and A.K. Niessen, *Cohesion in Metals*, North-Holland, Amsterdam, 1988.  
<sup>4</sup> B.E. Sundquist, *Acta Met.* **12** (1964) 67; W.L. Winterbottom and N.A. Gjostein, *Act. Met.* **14** (1966) 1041; J.C. Heyraud and J.J. Métois, *Acta Met.* **28** (1980) 1789; Z. Wang and P. Wynblatt, *Surf. Sci.* **398** (1998) 259.  
<sup>5</sup> U. Breuer and H.P. Bonzel, *Surf. Sci.* **273** (1992) 219.  
<sup>6</sup> J.C. Heyraud and J.J. Métois, *Surf. Sci.* **128** (1983) 334; J.C. Heyraud and J.J. Métois, *Surf. Sci.* **177** (1986) 213.  
<sup>7</sup> G. Bilalbegović, F. Ercolessi, and E. Tosatti, *Surf. Sci.* **280** (1993) 335; H.M. van Pixteren and J.W.M. Frenken, *Europhys. Lett.* **21** (1993) 43; H.M. van Pixteren, B. Pluis, and J.W.M. Frenken, *Phys. Rev. B* **49** (1994) 13798.  
<sup>8</sup> H.P. Bonzel and K. Dücker, *Surf. Sci.* **184** (1987) 425.  
<sup>9</sup> H.P. Bonzel and A. Edmundts, *Phys. Rev. Lett.* **84** (2000) 5804.  
<sup>10</sup> M. Methfessel, D. Hennig, and M. Scheffler, *Phys. Rev. B* **46** (1992) 4816.  
<sup>11</sup> H.L. Skriver and N.M. Rosengaard, *Phys. Rev. B* **46** (1992) 7157.  
<sup>12</sup> J. Kollár, L. Vitos, and H.L. Skriver, *Phys. Rev. B* **49** (1994) 11288.  
<sup>13</sup> C. Barreateau, D. Spanjaard, and M.C. Desjonquères, *Surf. Sci.* **433-435** (1999) 751.  
<sup>14</sup> M.M. Mehl and D. Papaconstantopoulos, *Phys. Rev. B* **54** (1996) 4519.  
<sup>15</sup> S.M. Foiles, M.I. Baskes, and M.S. Daw, *Phys. Rev. B* **33** (1996) 7983; G.J. Ackland, G. Tichy, V. Vitek, and M.W. Finnis, *Phil. Mag. A* **56** (1987) 735; D. Wolf, *Surf. Sci.* **226** (1990) 389; M.I. Baskes, *Phys. Rev. B* **46** (1992) 2727; P. van Beurden and G.J. Kramer, *Phys. Rev. B* **63** (2001) 165106.  
<sup>16</sup> A.M. Rodríguez, G. Bozzolo, and J. Ferrante, *Surf. Sci.* **289** (1993) 100.  
<sup>17</sup> P. Hohenberg and W. Kohn, *Phys. Rev.* **136** (1964) B864; W. Kohn and L.J. Sham, *Phys. Rev.* **140** (1965) A1133.  
<sup>18</sup> U. von Barth and L. Hedin, *J. Phys. C* **5** (1972) 1629.  
<sup>19</sup> H.L. Skriver and N.M. Rosengaard, *Phys. Rev. B* **43** (1991) 9538.  
<sup>20</sup> M. Alden, H.L. Skriver, S. Mirbt, and B. Johansson, *Phys. Rev. Lett.* **69** (1992) 2296; M. Alden, H.L. Skriver, S. Mirbt, and B. Johansson, *Sur. Sci.* **315** (1994) 157.  
<sup>21</sup> P.J. Feibelman, *Phys. Rev. B* **52** (1995) 16845.  
<sup>22</sup> L. Vitos, J. Kollár, and H.L. Skriver, *Phys. Rev. B* **55** (1997) 13521.  
<sup>23</sup> O.K. Andersen, and O. Jepsen, *Phys. Rev. Lett.* **53** (1984) 2671; O.K. Andersen, O. Jepsen, M. Sob, in: M. Yussouf (Ed.), *Electronic Band Structure and its Applications*, Springer-Berlin, 1987.  
<sup>24</sup> J.P. Perdew, K. Burke, and M. Ernzerhof, *Phys. Rev. Lett.* **77** (1996) 3865.  
<sup>25</sup> L. Vitos, A.V. Ruban, H.L. Skriver and J. Kollár, *Surf. Sci.* **411** (1998) 186.  
<sup>26</sup> L. Vitos, J. Kollár, and H.L. Skriver, *Phys. Rev. B* **49** (1994) 16694.  
<sup>27</sup> J.A. Moriarty and R. Phillips, *Phys. Rev. Lett.* **66** (1991) 3036.  
<sup>28</sup> L. Vitos, H.L. Skriver and J. Kollár, *Surf. Sci.* **425** (1999) 212.  
<sup>29</sup> I. Galanakis, G. Bihlmayer, V. Bellini, N. Papanikolaou, R. Zeller, S. Blügel, and P.H. Dederichs, *cond-mat/0105207*.  
<sup>30</sup> V. Bellini, N. Papanikolaou, R. Zeller, and P.H. Dederichs, *Phys. Rev. B* **64** (2001) 094403.  
<sup>31</sup> S.H. Vosko, L. Wilk, and N. Nusair, *Can. J. Phys* **58** (1980) 1200.  
<sup>32</sup> R. Zeller, P.H. Dederichs, B. Újfalussy, L. Szunyogh, and P. Weinberger, *Phys. Rev. B* **52** (1995) 8807; N. Papanikolaou, R. Zeller, and P.H. Dederichs, *J. Phys.: Cond. Matter*, to be published.  
<sup>33</sup> O.K. Andersen, Z. Pawłowska, and O. Jepsen, *Phys. Rev. B* **34** (1986) 5253.  
<sup>34</sup> N. Stefanou, H. Akai, and R. Zeller, *Comp. Phys. Commun.* **60** (1990) 231.  
<sup>35</sup> R. Zeller, *Phys. Rev. B* **55** (1997) 9400; K. Wildberger, R. Zeller, and P.H. Dederichs, *Phys. Rev. B* **55** (1997) 10074.

- <sup>36</sup> R. Zeller, J. Deutz, and P.H. Dederichs, *Sol. St. Comm.* **44** (1982) 993; K. Wildberger, P. Lang, R. Zeller, and P.H. Dederichs, *Phys. Rev. B* **52** (1995) 11502.
- <sup>37</sup> H.J. Monkhorst and J.D. Pack, *Phys. Rev. B* **13** (1976) 5188.
- <sup>38</sup> N.W. Ashcroft and N. D. Mermin, *Solid State Physics*, Saunders College Publishing, 1976.
- <sup>39</sup> J.K. Mackenzie, A.J.W. Moore, and J.F. Nicholas, *J. Phys. Chem. Solids* **23** (1962) 185 .
- <sup>40</sup> P.J. Feibelman and D.R. Hamann, *Surf. Sci.* **234** (1990) 377.
- <sup>41</sup> P.J. Feibelman, *Phys. Rev. B* **46** (1992) 2532.
- <sup>42</sup> M. Mansfield and R.J. Needs, *Phys. Rev. B* **43** (1991) 8829.
- <sup>43</sup> J. Wan, Y.L. Fan, D.W. Gong, S.G. Shen, and X.Q. Fan, *Modelling Simul. Mater. Sci. Eng.* **7** (1999) 189; and references therein.
- <sup>44</sup> N.D. Lang and W. Kohn, *Phys. Rev. B* **1** (1970) 4555; J.P. Perdew and R. Monniert, *Phys. Rev. Lett.* **37** (1976) 1286; R. Monniert and J.P. Perdew, *Phys. Rev. B* **17** (1978) 2595; Z.Y. Zhang, D.C. Langreth, and J.P. Perdew, *Phys. Rev. B* **41** (1990) 5674; J.P. Perdew, H.Q. Tran, and E. Smith, *Phys. Rev. B* **42** (1990) 11627; K.F. Wojciechowski, *Surf. Sci.* **437** (1999) 285.
- <sup>45</sup> J. Schöchlin, K.. Bohnen, and K.M. Ho, *Surf. Sci.* **324** (1995) 113.
- <sup>46</sup> R. Stumpf and M. Scheffler, *Phys. Rev. B* **53** (1996) 4958.
- <sup>47</sup> Th. Rodach, K.P. Bohnen, and K.M. Ho, *Surf. Sci.* **286** (1993) 66.
- <sup>48</sup> H.M. Polatoglou, M. Methfessel, and M. Scheffler, *Phys. Rev. B* **48** (1993) 1877.
- <sup>49</sup> H. Bross and M. Kauzmann, *Phys. Rev. B* **51** (1995) 17135.
- <sup>50</sup> A. Eichler, J. Hafner, J. Furthmüller, and G. Kresse, *Surf. Sci.* **346** (1996) 300.
- <sup>51</sup> L. Morrison, D.M. Bylander, and L. Kleinman, *Phys. Rev. Lett.* **71** (1993) 1083.
- <sup>52</sup> M. Weinert, R.E. Watson, J.W. Davenport, and G.W. Fernando, *Phys. Rev. B* **39** (1989) 12585.
- <sup>53</sup> A. Wachter, K.P. Bohnen, and K.M. Ho, *Surf. Sci.* **346** (1996) 127.
- <sup>54</sup> H. Erschbaumer, A.J. Freeman, C.L. Fu, and R. Podloucky, *Surf. Sci.* **243** (1991) 317.
- <sup>55</sup> N. Takeuchi, C.T. Chan, and K.M. Ho, *Phys. Rev. B* **43** (1991) 14363.
- <sup>56</sup> R.J. Needs and M. Mansfield, *J. Phys.: Condens. Matter* **1**, (1989) 7555.
- <sup>57</sup> N. Takeuchi, C.T. Chan, and K.M. Ho, *Phys. Rev. B* **43** (1991) 13899.
- <sup>58</sup> R. Eibler, H. Erschbaumer, C. Temnitschka, R. Podloucky, and A.J. Freeman, *Surf. Sci.* **280** (1993) 398.
- <sup>59</sup> K.M. Ho and K.P. Bohnen, *Phys. Rev. Lett.* **59** (1987) 1833.

TABLE I. Scalar-relativistic surface energies and anisotropy ratios in parenthesis for Ag within ASA using different values for the  $\ell_{max}$  cut-off (LM), the tight-binding cluster (TB), the number of energy points (EN) to perform integrations in the complex energy plane and the number of  $\mathbf{k}_{\parallel}$ -points in the full two-dimensional Brillouin zone. The first set of parameters is the one used in the present calculations.

LM	TB	EN	KP	Ag(111)	Ag(100)	Ag(110)
3	19	27	55×55	0.641	(1.34) 0.860	(1.98) 1.271
3	55	27	55×55	0.637	(1.34) 0.854	(1.98) 1.262
3	19	41	55×55	0.643	(1.33) 0.855	(1.97) 1.266
3	19	27	75×75	0.648	(1.33) 0.860	(1.96) 1.273
3	55	41	75×75	0.642	(1.32) 0.849	(1.96) 1.259
4	19	27	55×55	0.649	(1.35) 0.879	(2.00) 1.301

TABLE II. Effect of lattice parameter changes on the scalar-relativistic ASA surface energies for the three low-index surfaces of Cu in the upper panel and for the (111) surface of Cu, Ag and Au in the bottom panel,

		Cu(111)		Cu(100)		Cu(110)	
$\frac{a_{exp}-a}{a_{exp}}$	$\gamma$ (eV)	$\frac{\gamma_{exp}-\gamma}{\gamma_{exp}}$	$\gamma$ (eV)	$\frac{\gamma_{exp}-\gamma}{\gamma_{exp}}$	$\gamma$ (eV)	$\frac{\gamma_{exp}-\gamma}{\gamma_{exp}}$	
0%	0.737		0.982		1.455		
1%	0.730	0.95%	0.971	1.12%	1.441	0.96%	
2%	0.719	2.44%	0.956	2.65%	1.420	2.41%	
3%	0.706	4.21%	0.939	4.38%	1.394	4.19%	
		Cu(111)		Ag(111)		Au(111)	
$\frac{a_{exp}-a}{a_{exp}}$	$\gamma$ (eV)	$\frac{\gamma_{exp}-\gamma}{\gamma_{exp}}$	$\gamma$ (eV)	$\frac{\gamma_{exp}-\gamma}{\gamma_{exp}}$	$\gamma$ (eV)	$\frac{\gamma_{exp}-\gamma}{\gamma_{exp}}$	
0%	0.737		0.641		0.755		
1%	0.730	0.95%	0.636	0.78%	0.739	2.12%	
2%	0.719	2.44%	0.624	2.65%	0.717	5.03%	
3%	0.706	4.21%	0.609	4.99%	0.692	8.34%	

TABLE III. Full-potential scalar-relativistic surface energies for the six more closed-packed surfaces for the four transition metals. In parenthesis the anisotropy ratios with respect to the (111) surface.

$\gamma$ (eV)	Pd	Pt	Rh	Ir
(111)	0.822	0.957	1.034	1.200
(100)	(1.28) 1.049	(1.33) 1.272	(1.36) 1.404	(1.42) 1.707
(110)	(1.94) 1.596	(2.06) 1.973	(1.98) 2.047	(2.07) 2.488
(113)	(2.28) 1.873	(2.40) 2.295	(2.35) 2.428	(2.43) 2.913
(331)	(2.93) 2.404	(2.98) 2.853	(2.99) 3.094	(3.04) 3.652
(210)	(3.22) 2.644	(3.30) 3.158	(3.35) 3.464	(3.48) 4.172



TABLE IV. Surface energies is  $\text{J m}^{-2}$  for the three low-index surfaces of the paramagnetic fcc transition metals using the FKRR. In second column the results using the FCD-LMTO-ASA and on the third and fourth columns existing *ab-initio* calculations and experiments.

$\gamma$ ( $\text{J m}^{-2}$ )	FKRR	Ref. 25	Other Calc.	Experiments	
Cu	(111)	1.91	1.95	1.59 <sup>c</sup> , 1.94 <sup>d</sup>	1.79 <sup>a</sup> , 1.83 <sup>b</sup>
	(100)	2.15	2.17	1.71 <sup>c</sup> , 1.80 <sup>e</sup>	
	(110)	2.31	2.24	1.85 <sup>c</sup>	
Rh	(111)	2.65	2.47	2.53 <sup>f</sup> , 2.85 <sup>g</sup>	2.66 <sup>a</sup> , 2.70 <sup>b</sup>
	(100)	3.12	2.80	2.81 <sup>f</sup> , 3.28 <sup>g</sup> , 2.65 <sup>h</sup> , 2.59 <sup>i</sup>	
	(110)	3.22	2.90	2.88 <sup>f</sup> , 3.37 <sup>g</sup>	
Pd	(111)	2.01	1.92	1.64 <sup>f</sup>	2.00 <sup>a</sup> , 2.05 <sup>b</sup>
	(100)	2.22	2.33	1.86 <sup>f</sup> , 2.30 <sup>j</sup> , 2.13 <sup>k</sup>	
	(110)	2.39	2.23	1.97 <sup>f</sup> , 2.50 <sup>j</sup>	
Ag	(111)	1.25	1.17	1.21 <sup>f</sup>	1.25 <sup>a</sup> , 1.25 <sup>b</sup>
	(100)	1.40	1.20	1.21 <sup>f</sup> , 1.30 <sup>j</sup> , 1.27 <sup>l</sup> , 1.11 <sup>m</sup>	
	(110)	1.51	1.24	1.26 <sup>f</sup> , 1.40 <sup>j</sup>	
Ir	(111)	3.02	2.97	3.27 <sup>n</sup>	3.05 <sup>a</sup> , 3.00 <sup>b</sup>
	(100)	3.71	3.72		
	(110)	3.82	3.61		
Pt	(111)	2.31	2.30	2.20 <sup>n</sup> , 2.07 <sup>o</sup>	2.49 <sup>a</sup> , 2.48 <sup>b</sup>
	(100)	2.65	2.73		
	(110)	2.91	2.82		
Au	(111)	1.39	1.28	1.25 <sup>m</sup> , 1.04 <sup>p</sup>	1.51 <sup>a</sup> , 1.50 <sup>b</sup>
	(100)	1.62	1.63	1.33 <sup>m</sup> , 1.30 <sup>q</sup>	
	(110)	1.75	1.70	1.43 <sup>r</sup>	

- <sup>a</sup> Experiment, Ref. 2; <sup>b</sup> Experiment, Ref. 3  
<sup>c</sup> Pseudopotentials, Ref. 47; <sup>d</sup> FP-LMTO, Ref. 48  
<sup>e</sup> modified APW, Ref. 49; <sup>f</sup> FP-LMTO, Ref. 10  
<sup>g</sup> Pseudopotentials, Ref. 50; <sup>h</sup> Pseudopotentials, Ref. 51  
<sup>i</sup> FLAPW, Ref. 40; <sup>j</sup> FLAPW, Ref. 52  
<sup>k</sup> Pseudopotentials, Ref. 53; <sup>l</sup> FLAPW, Ref. 54  
<sup>m</sup> Pseudopotentials, Ref. 55; <sup>n</sup> Pseudopotentials, Ref. 56  
<sup>o</sup> Pseudopotentials, Ref. 21; <sup>p</sup> Pseudopotentials, Ref. 57  
<sup>q</sup> FLAPW, Ref. 58; <sup>r</sup> Pseudopotentials, Ref. 59

TABLE V. Full-potential scalar-relativistic surface energies for the six more closed-packed surfaces of the four *sp* metal. In parenthesis the anisotropy ratios with respect to the (111) surface.

$\gamma$ (eV)	Ca	Sr	Al	Pb
(111)	0.417	0.373	0.489	0.398
(100)	(1.21) 0.503	(1.22) 0.454	(1.28) 0.625	(1.24) 0.492
(110)	(1.92) 0.797	(1.94) 0.722	(1.93) 0.943	(1.95) 0.778
(311)	(2.27) 0.946	(2.27) 0.847	(2.24) 1.094	(2.18) 0.866
(331)	(2.96) 1.234	(2.93) 1.094	(2.94) 1.436	(2.81) 1.118
(210)	(3.20) 1.333	(3.18) 1.187	(3.20) 1.565	(3.53) 1.405

TABLE VI. Surface energies is  $\text{J m}^{-2}$  for the three low-index surfaces of the paramagnetic fcc *sp* metals using the FKRR. In second column the results using the FCD-LMTO-ASA and on the third and fourth columns existing *ab-initio* calculations and experiments.

$\gamma$ ( $\text{J m}^{-2}$ )	FKRR	Ref. 25	Other Calc.	Experiments
Ca (111)	0.50	0.57		0.50 <sup>a</sup> , 0.49 <sup>b</sup>
Ca (100)	0.52	0.54		
Ca (110)	0.58	0.58		
Sr (111)	0.37	0.43		0.42 <sup>a</sup> , 0.41 <sup>b</sup>
Sr (100)	0.39	0.41		
Sr (110)	0.44	0.43		
Al (111)	1.10	1.12	0.94 <sup>c</sup> , 1.12 <sup>d</sup>	1.14 <sup>a</sup> , 1.12 <sup>b</sup>
Al (100)	1.22	1.35	1.08 <sup>c</sup> , 1.14 <sup>d</sup>	
Al (110)	1.30	1.27	1.09 <sup>c</sup> , 1.28 <sup>d</sup>	
Pb (111)	0.60	0.32	0.50 <sup>e</sup>	0.59 <sup>a</sup> , 0.60 <sup>b</sup>
Pb (100)	0.64	0.38		
Pb (110)	0.72	0.45	0.59 <sup>e</sup>	

<sup>a</sup> Experiment, Ref. 2; <sup>b</sup> Experiment, Ref. 3

<sup>c</sup> Pseudopotentials, Ref. 45; <sup>d</sup> Pseudopotentials, Ref. 46

<sup>e</sup> Pseudopotentials, Ref. 42

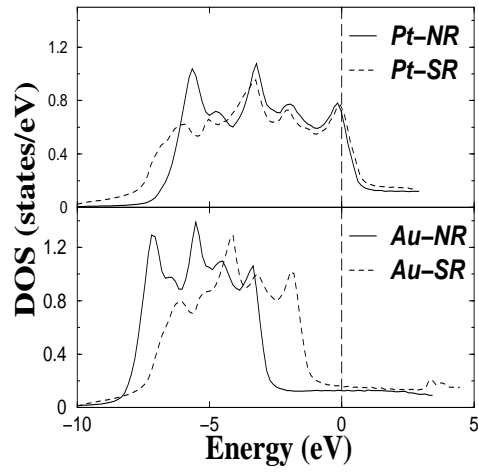


FIG. 1. Non-relativistic (NR) density of states (DOS) of Pt (upper panel) and Au (bottom panel) compared with the scalar-relativistic (SR) DOS. All DOSs are calculated for the central layer atom of the (111) slab.

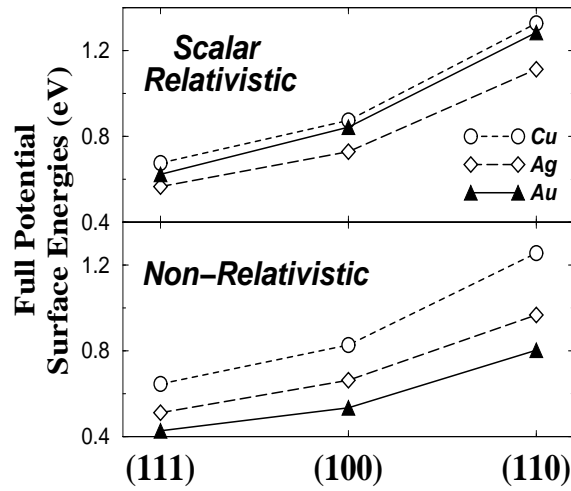


FIG. 2. Effect of relativity on the full-potential surface energies of the noble metals. The effect of relativity is large for Au that possesses  $5d$  electrons. Relativity also enhances the anisotropy ratios.

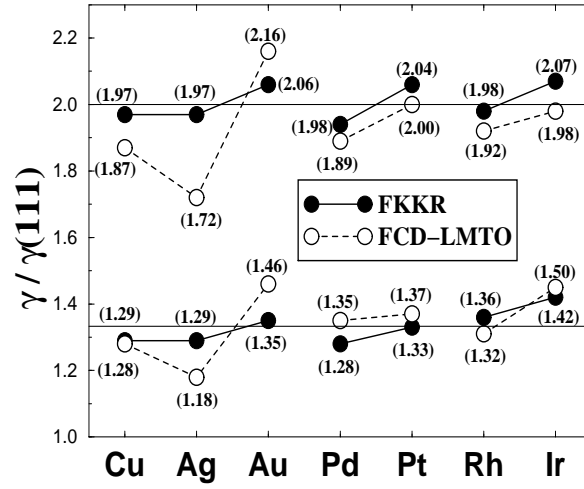


FIG. 3. Anisotropy ratios within both FKKR and LMTO from reference 25. Contrary to the noble metals, whose (111) surface possesses a surface state centered at the  $\bar{\Gamma}$  point, the transition metals results are similar for both methods.

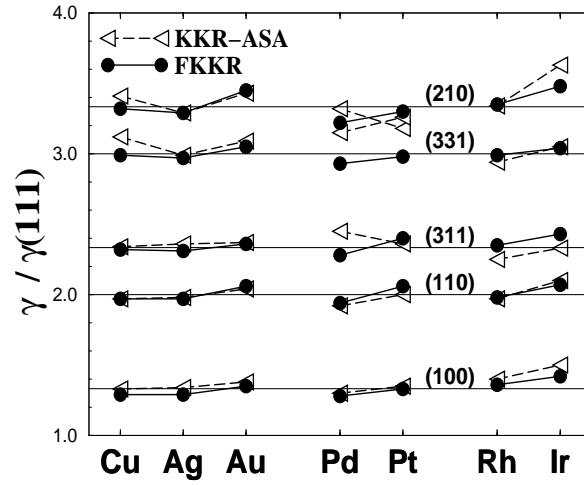


FIG. 4. Anisotropy ratios for the low-index and the most close-packed vicinal surfaces within ASA and FP. For the vicinal surfaces the use of FP is necessary, due to the failure of ASA to describe accurately the more complex metal-vacuum interface.

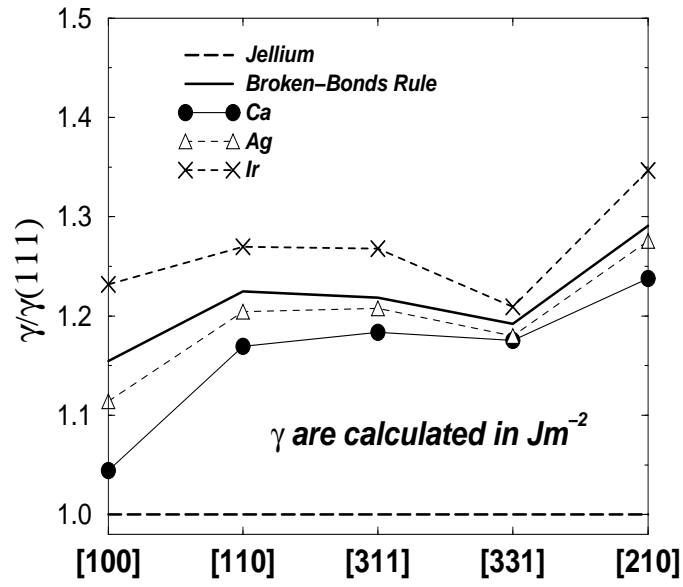


FIG. 5. Anisotropy ratios but calculating the surface energies in  $\text{Jm}^{-2}$  for Ag, Ir and Ca. The solid line corresponds to the broken-bon rule and the tilted one to the jellium. The Ca(100) surface is close to jellium but then it recovers the Ag and Ir behavior.